Archive of Applied Mechanics (2022) 92:1953–1971
https://doi.org/10.1007/s00419-022-02159-5

ORIGINAL

Murat Yaylacı · Merve Abanoz · Ecren Uzun Yaylacı · Hasan Ölmez · Dursun Murat Sekban · Ahmet Birinci

Evaluation of the contact problem of functionally graded layer resting on rigid foundation pressed via rigid punch by analytical and numerical (FEM and MLP) methods

Received: 22 February 2022 / Accepted: 1 April 2022 / Published online: 20 April 2022

Abstract In this paper, frictionless contact problem for a functionally graded (FG) layer is considered. The FG layer is subjected to load with a rigid punch and the FG layer is bonded on a rigid foundation. Analysis of this contact problem was carried out by analytical method, finite element method (FEM) and multilayer perceptron (MLP), comparatively. The main target of this study is to investigate the applicability of MLP analysis for frictionless contact problem of FG layer bonded on a rigid foundation. Analytical solution of the problem is based on the theory of elasticity and integral transform techniques. The physical contact problem is transformed to mathematical system of integral equation. The integral equation in which the contact pressures are unknown functions is numerically solved with the Gauss–Jacobi integration formulation. Finite element analysis of the problem is carried out with ANSYS software by using the two-dimensional modeling technique. Finally, MLP analysis has been used to obtain the contact distances of the problem. Three-layer MLP was used for this calculation. Material properties and loading conditions were created by giving examples of different values in MLP training and testing stages. Program code was rewritten in C++. As a result, average deviation values such as 1.67 and 0.885 were obtained for FEM and MLP, respectively. It has been determined that the contact areas and contact stresses obtained from FEM and MLP are quite compatible with the results obtained from the analytical method.

Keywords Theory of elasticity · Finite element method · Multilayer perceptron · Functionally graded layer · Contact mechanics

M. Yaylacı (✉)
Department of Civil Engineering, Recep Tayyip Erdogan University, 53100 Rize, Turkey
e-mail: murat.yaylaci@erdogan.edu.tr

M. Abanoz
Department of Construction Technology, Kastamonu University, 37100 Kastamonu, Turkey
e-mail: merveabanoz@kastamonu.edu.tr

E. U. Yaylacı
Surmene Faculty of Marine Science, Karadeniz Technical University, 61040 Trabzon, Turkey
e-mail: ecren.uzun@ktu.edu.tr

H. Ölmez · D. M. Sekban
Department of Marine Engineering Operations, Karadeniz Technical University, 61040 Trabzon, Turkey
e-mail: hasanolmez@ktu.edu.tr

D. M. Sekban
e-mail: msekban@ktu.edu.tr

A. Birinci
Department of Civil Engineering, Karadeniz Technical University, 61080 Trabzon, Turkey
e-mail: birinci@ktu.edu.tr

1 Introduction

The subject of contact mechanics is a fundamental field of study to investigate and understand the deformation and wear mechanisms of solids that interact with each other due to a contact zone. For these studies, an engineer must design contacting components by first doing a stress analysis of the contacting elements in order to determine the effect of physical interaction types and structural behavior under stationary or dynamic contact. Structural behavior and life assessment of the engineering system including two or more solid bodies are brought into contact under static, and dynamic or cyclic loads are indispensable for a structural analysis. In any kind of contact, the surface and the subsurface stresses should be determined in order to decrease the damaging effects such as wear, fatigue, fracture, and collapse. Therefore, determining the contact stress distribution in the contact zone with a fast and reliable method has recently become an important phenomenon [1, 2].

Functionally graded materials (FGM) contact mechanic is one of the challenging subjects of this phenomenon. FGMs are engineered materials produced to show a specific performance with spatial grading in their structure and/or composition [3]. FGMs belong to composite materials class whose mechanical properties vary continuously from one surface to another at macro-level [4]. The ability to obtain special morphologies and mechanical properties in the desired direction makes functionally graded materials advantageous among composite materials [5–9]. Because of these advantages, the use of functionally graded materials is increasing day by day in many different sectors. This increase in usage has recently led to the increase in studies on the contact mechanics of FDMs. Studies on the contact mechanics of functionally graded materials are summarized below. The contact problem of FG layer fitting to homogeneous two quarter planes and a rigid plane was examined by Adiyaman et al. [10]. Yan and Mi [11] have aimed to analyze the receding contact between a homogeneous elastic layer and a half plane reinforced by a functionally graded coating. Comez [12] has obtained the fundamental formulation for the continuous and discontinuous contact problems of a functionally graded layer pressed by a rigid cylindrical punch lying on a rigid substrate without using superposition technique. Contact problems of FGMs for different geometries and loading cases have been investigated by researchers using analytical solutions through the theory of elasticity and numerical solutions through the finite element method [13, 14].

A limited number of contact problems are sufficiently well behaved to have an analytical solution. For this reason, contact problems are solved with numerical techniques in general. The most used technique to treat structural nonlinearities is the FEM. There are important studies for concrete structural analysis using FEM method in civil engineering literature [15–21]. Oner et al. [22] have investigated the continuous and discontinuous contact problem of layer under the pressure influence by using FEM. Lezgy-Nazargah and Meshkani [23] have developed a four-node quadrilateral partial mixed plate element with low degrees of freedom for static and free vibration analysis of FGM plates rested on Winkler Pasternak elastic foundations. Yaylaci et al. [24–26] have examined the FEM analysis of contact problem of the functionally graded layer.

The meanings of the contact parameters such as normal contact stiffness, penetration limit, and the contact algorithms in FEM software are depending on the user experience with contact problems. An alternative used in this work to avoid experimentation is to employ artificial neural networks (ANNs), where some results of the contact solution are used to estimate the contact parameters. In this study, multilayer perceptron (MLP), a class of feedforward artificial neural network, is used. There are precious works for civil engineering analysis using MLP analysis in the literature [27–29] that have examined the contact stiffness estimation in ANSYS using simplified models and artificial neural networks. Serafińska et al. [30] have used ANN in their study about friction law for elastomeric materials applied in finite element sliding contact simulations. Górski et al. [31] have studied the identification of the stick and slip motion between contact surfaces using the ANN structure. Researchers have examined the analytical and numerical (ANN) analysis of contact problem [32–35].

In the literature, it appears that shear modulus of the FG layer is changed depending on an exponential function. Generally, the effect of the material stiffness parameter on the contact stress and contact length was investigated. The distinctive feature of this study from similar studies in the literature is that the loading in the problem and geometry are applied differently. In this study, a frictionless contact problem between a rigid punch and functionally graded (FG) layer, which is bonded to a rigid foundation on its bottom surface was investigated by using the analytical method (theory of elasticity), FEM and multilayer perceptron. The layer considered in the problem is functionally graded (FG) and its shear modulus is assumed to vary exponentially through the thickness of the layer. Dimensionless contact stresses between FG layer and half plane were obtained for the various dimensionless quantities. All results of these methods were compared to each other.

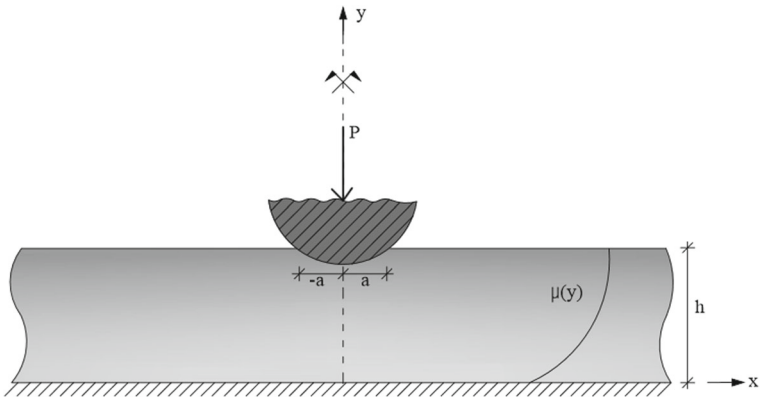

Fig. 1 Geometry and loading of the contact problem

2 Theoretical solution

General expressions of stresses and displacements are briefly and firstly obtained by using the fundamental equations of theory of elasticity and integral transformation technique. After the description of the problem, a set of linear algebraic equation is obtained by applying the expressions of stresses and displacements to boundary conditions of the problem. By solving the equations system, the unknown constant coefficients are expressed depending on the contact pressure which is unknown. Using the condition that is derivative of vertical displacements under the rigid punch is equal to derivative of the function $F(x)$ which defines the profile of the rigid punch, and the problem is formulated in terms of a singular integral equation for the contact problem. The singular integral equation is solved numerically by using Gauss–Jacobi integration formulation and the contact areas, and the contact pressure is determined.

The solution of the contact problem of a layered resting on rigid foundation is considered. The loading and the geometry of the problem are given in Fig. 1 representatively. The problem consists of an infinitely long functionally graded (FG) layer which bonded to a rigid support on its lower surface. The thickness of FG layer is h and a concentrated force P is the layer via a rigid cylindrical punch with radius R. Poisson's ratio ν is taken as constant, the shear modulus μ depends on the y-coordinate only as follows:

$$\mu(y) = \mu_0 e^{\beta y}, \quad 0 \le y \le h \tag{1}$$

where μ_0 is the shear modulus of the graded layer at $y = 0$, β is the non-homogeneity parameter controlling the variation of the shear modulus in the graded layer. It is assumed that the contact surfaces are frictionless and $x = 0$ is to be the plane of symmetry with respect to external loads as well as geometry, for simplicity. Clearly, it is enough to consider one half (i.e., $x \ge 0$) of the medium only.

Assuming that the FG layer is isotropic at every point, equilibrium equations, the strain–displacement relationships, and the linear elastic stress–strain law, respectively, are given by:

$$\frac{\partial \sigma_x}{\partial x} + \frac{\tau_{xy}}{\partial y} = 0, \quad \frac{\partial \tau_{yx}}{\partial x} + \frac{\partial \sigma_y}{\partial y} = 0 \tag{2}$$

$$\varepsilon_{xx} = \frac{\partial u}{\partial x}, \quad \varepsilon_{yy} = \frac{\partial v}{\partial y}, \quad \varepsilon_{xy} = \frac{1}{2}\left(\frac{\partial u}{\partial y} + \frac{\partial v}{\partial x}\right) \tag{3}$$

$$\sigma_x = \frac{\mu(y)}{\kappa - 1}\left[(1+\kappa)\varepsilon_{xx} + (3-\kappa)\varepsilon_{yy}\right] \tag{4a}$$

$$\sigma_y = \frac{\mu(y)}{\kappa - 1}\left[(3-\kappa)\varepsilon_{xx} + (1+\kappa)\varepsilon_{yy}\right] \tag{4b}$$

$$\tau_{xy} = 2\mu(y)\varepsilon_{xy} \tag{4c}$$

where u and v are the x and y components of the displacement field, respectively; σ_x, σ_y, and τ_{xy} are the components of the stress field in the same coordinate system; ε_x, ε_y, and ε_{xy} are the corresponding components

of the strain field; κ is a material property defined as $\kappa = 3 - 4\nu$ for plane-strain problems. Combining Eqs. (1)-(4), the following two-dimensional Navier equations are obtained:

$$(\kappa+1)\frac{\partial^2 u}{\partial x^2} + (\kappa-1)\frac{\partial^2 u}{\partial y^2} + 2\frac{\partial^2 v}{\partial x \partial y} + \beta(\kappa-1)\frac{\partial u}{\partial y} + \beta(\kappa-1)\frac{\partial v}{\partial x} = 0 \tag{5a}$$

$$(\kappa-1)\frac{\partial^2 v}{\partial x^2} + (\kappa+1)\frac{\partial^2 v}{\partial y^2} + 2\frac{\partial^2 u}{\partial x \partial y} + \beta(3-\kappa)\frac{\partial u}{\partial x} + \beta(\kappa+1)\frac{\partial v}{\partial y} = 0. \tag{5b}$$

In case of graded layer solution, using symmetry considerations and Fourier transforms, the displacement components for FG layer may be written:

$$u_h(x,y) = \frac{2}{\pi}\int_0^\infty \phi(\xi,y)\sin(\xi x)\mathrm{d}\xi, \quad v_h(x,y) = \frac{2}{\pi}\int_0^\infty \psi(\xi,y)\cos(\xi x)\mathrm{d}\xi \tag{6}$$

where $\phi(\xi, y)$ and $\psi(\xi, y)$ are the inverse Fourier sine and Fourier cosine transforms of u and v with respect to the x-coordinate and the y-coordinate, respectively. By substituting Eq. (6) into Navier Eq. (5), the following ordinary differential equations are obtained:

$$-(\kappa+1)\xi^2\phi + (\kappa-1)\frac{\mathrm{d}^2\phi}{\mathrm{d}y^2} - 2\xi\frac{\mathrm{d}\psi}{\mathrm{d}y} + \beta(\kappa-1)\left[\frac{\mathrm{d}\phi}{\mathrm{d}y} - \xi\psi\right] = 0 \tag{7a}$$

$$-(\kappa-1)\xi^2\psi + (\kappa+1)\frac{\mathrm{d}^2\psi}{\mathrm{d}y^2} + 2\xi\frac{\mathrm{d}\phi}{\mathrm{d}y} + \beta\left[(3-\kappa)\xi\phi + (\kappa+1)\frac{\mathrm{d}\psi}{\mathrm{d}y}\right] = 0 \tag{7b}$$

where

$$\phi = \sum_{j=1}^{4} A_j e^{n_j y}, \quad \psi = \sum_{j=1}^{4} A_j m_j e^{n_j y} \tag{8}$$

The unknown functions $A_j (j = 1,2,3,4)$ are determined from the boundary conditions and $n_1,\ldots n_4$ are the four complex roots of the characteristic equation associated with Eq. (7a, b), which may be written:

$$n_j^4 + 2\beta n_j^3 + (\beta^2 - 2\xi^2)n_j^2 - 2\xi^2\beta n_j + \xi^2\left(\xi^2 + \beta^2\frac{3-\kappa}{\kappa+1}\right) = 0. \tag{9}$$

The roots of Eq. (9) are obtained:

$$n_1 = -\frac{1}{2}\left(\beta + \sqrt{4\xi^2 + \beta^2 - 4\xi\beta i\sqrt{\frac{3-\kappa}{\kappa+1}}}\right), \quad n_2 = -\frac{1}{2}\left(\beta - \sqrt{4\xi^2 + \beta^2 - 4\xi\beta i\sqrt{\frac{3-\kappa}{\kappa+1}}}\right) \tag{10a}$$

$$n_3 = -\frac{1}{2}\left(\beta + \sqrt{4\xi^2 + \beta^2 + 4\xi\beta i\sqrt{\frac{3-\kappa}{\kappa+1}}}\right), \quad n_4 = -\frac{1}{2}\left(\beta - \sqrt{4\xi^2 + \beta^2 + 4\xi\beta i\sqrt{\frac{3-\kappa}{\kappa+1}}}\right). \tag{10b}$$

The known function m_j in Eq. (8) may be expressed as follows:

$$m_j = \frac{(3\beta + 2n_j - \beta\kappa)\left[n_j(\beta + n_j)(\kappa+1) - \xi^2(\kappa+3)\right]}{\xi\left[4\xi^2 - \beta^2(\kappa-3)(\kappa+1)\right]}, \quad (j = 1,\ldots,4). \tag{11}$$

By substituting Eqs. (6,8) into Eq. (4), stress and displacement fields of interest for graded layer are obtained:

$$\sigma_{y_h} = \frac{2\mu_0 e^{(\beta y)}}{\pi(\kappa-1)}\int_0^\infty \sum_{j=1}^{4} A_j C_j e^{(n_j y)}\cos(\xi x)\mathrm{d}\xi \tag{12a}$$

$$\tau_{xy_h} = \frac{2\mu_0 e^{(\beta y)}}{\pi}\int_0^\infty \sum_{j=1}^{4} A_j D_j e^{(n_j y)}\sin(\xi x)\mathrm{d}\xi \tag{12b}$$

$$v_h = \frac{2}{\pi}\int_0^\infty \sum_{j=1}^{4} A_j m_j e^{(n_j y)} \cos(\xi x)\mathrm{d}\xi \tag{12c}$$

$$u_h = \frac{2}{\pi}\int_0^\infty \sum_{j=1}^{4} A_j e^{(n_j y)} \sin(\xi x)\mathrm{d}\xi \tag{12d}$$

in which the known functions C_j and $D_j (j = 1,2,3,4)$ are given by:

$$C_j = (3-\kappa)\xi + (\kappa+1)m_j n_j, \quad D_j = n_j - \xi m_j. \tag{13}$$

The boundary conditions of the contact problem for the FG layer can be written as,

$$u(x,0) = 0, \quad (0 \le x < \infty) \tag{14a}$$

$$v(x,0) = 0, \quad (0 \le x < \infty) \tag{14b}$$

$$\tau_{xy}(x,h) = 0, \quad (0 \le x < \infty) \tag{14c}$$

$$\sigma_y(x,h) = \left\{ \begin{matrix} -p(x); & (0 \le x < a) \\ 0; & (0 \le x < \infty) \end{matrix} \right\} \tag{14d}$$

$$\frac{\partial}{\partial x}[v(x,h)] = f(x), \quad (0 \le x < a)a \tag{15}$$

where $p(x)$ is the unknown contact stress between the rigid punch and the layer on the contact area $(-a,a)$ and $f(x)$ is the derivative of the profile of the rigid punch; one may write

$$f(x) = \frac{x}{R}. \tag{16}$$

By applying boundary conditions (14) to Eq. (12), the following linear algebraic system of equations is obtained:

$$\tau_{xy}(x,h) = 0, \quad \sum_{j=1}^{4} A_j D_j e^{n_j y} = 0 \tag{17a}$$

$$\sigma_y(x,h) = -p(x), \quad \sum_{j=1}^{4} A_j C_j e^{n_j y} = -P \tag{17b}$$

$$v(x,0) = 0, \quad \sum_{j=1}^{4} A_j m_j = 0 \tag{17c}$$

$$u(x,0) = 0, \quad \sum_{j=1}^{4} A_j = 0 \tag{17d}$$

$$\begin{bmatrix} D_1 e^{(n_1 h)} & D_2 e^{(n_2 h)} & D_3 e^{(n_3 h)} & D_4 e^{(n_4 h)} \\ C_1 e^{(n_1 h)} & C_2 e^{(n_1 h)} & C_3 e^{(n_1 h)} & C_4 e^{(n_1 h)} \\ m_1 & m_2 & m_3 & m_4 \\ 1 & 1 & 1 & 1 \end{bmatrix} \begin{Bmatrix} A_1 \\ A_2 \\ A_3 \\ A_4 \end{Bmatrix} = \begin{Bmatrix} 0 \\ -P \\ 0 \\ 0 \end{Bmatrix} \tag{17e}$$

where P is the known function defined as:

$$P = \frac{(\kappa_1 - 1)}{\mu_0 e^{\beta h}} \int_0^\infty p(x)\cos(\xi x)\mathrm{d}x. \tag{18}$$

The unknown functions $A_j = (j = 1, 2, 3, 4)$ are obtained:

$$A_j = \frac{A_{j1}}{\Delta A} P \tag{19}$$

where $A_j (j = 1,2,3,4)$ and ΔA are shown in Appendix 1. Substituting them into the rested boundary condition (12) and using the symmetry consideration, $p(x) = p(-x)$, and some routine manipulations.

$$\frac{2}{\pi \mu_0 e^{\beta h}} \int_{-a}^{a} \left[\frac{\kappa + 1}{8} \left(\frac{1}{x - t} \right) + N(x, t) \right] p(t) \mathrm{d}t = \frac{x}{R} \tag{20}$$

where $N(x,t)$ is given in Appendix 2. In the singular integral Eq. (20), the contact area a is also unknown, as well as the contact stress $p(x)$. For a complete solution of the problem, the contact stress $p(x)$ must satisfy the following equilibrium condition:

$$\int_{-a}^{a} p(t) \mathrm{d}t = P. \tag{21}$$

To simplify the numerical analysis of the integral equation, the following dimensionless quantities can be introduced.

$$t = ar, \quad \mathrm{d}t = a\mathrm{d}r \tag{22a}$$

$$x = as \tag{22b}$$

$$z = \xi h, \quad \mathrm{d}z = h\mathrm{d}\xi \tag{22c}$$

$$\phi(r) = \frac{h}{P} P(t). \tag{22d}$$

By using these dimensionless quantities, the integral Eqs. (20) and (21) can be written as follows.

$$\int_{-1}^{1} \left[\frac{\kappa + 1}{8} \frac{1}{s - r} + \frac{a}{h} k(s, r) \right] \phi(r) \mathrm{d}r = \frac{\pi e^{\beta h}}{2R/h} \frac{\mu_0}{P/h} \frac{a}{h} s \tag{23a}$$

$$\frac{a}{h} \int_{-1}^{1} \phi(r) \mathrm{d}r = 1 \tag{23b}$$

where $k(s,r)$ is given in Appendix 3. The solution of the integral equations can be expressed as,

$$\phi(r) = w(r) g(r). \tag{24a}$$

Since there are smooth contacts at the end points, the index of the integral Eq. (23a) is (-1) [36].

$$w(r) = (1 - r)^{\alpha} (1 + r)^{\beta}, \quad (\alpha = 0.5, \beta = 0.5). \tag{24b}$$

The solution of the integral equation can be expressed as follows by using the Gauss–Jacobi integration formulas, the integral Eq. (23a) and equilibrium conditions (23b) become,

$$\sum_{i=1}^{N} W_i^N g(r_i) \left[\frac{\kappa + 1}{8} \frac{1}{s_k - r_i} + \frac{a}{h} k(s_k, r_i) \right] = \frac{\pi e^{\beta h}}{2} \frac{\mu_0}{P/h} \frac{a/h}{R/h} s_k, \quad k(1, \ldots, N + 1) \tag{25a}$$

$$\frac{a}{h} \sum_{i=1}^{N} W_i(r_i) g(r_i) = 1. \tag{25b}$$

r_i and s_k are the roots of the related Jacobi polynomials and W_i^N is the weighting constant

$$r_i = \cos\left(\frac{i\pi}{N + 1} \right), \quad (i = 1, \ldots N) \tag{26a}$$

$$s_k = \cos\left(\frac{\pi}{2} \frac{2k - 1}{N + 1} \right), \quad (k = 1, \ldots N + 1) \tag{26b}$$

Table 1 Test parameters

β	κ	$\frac{\mu_0}{P/h}$	R/h
−1	1.5	50	10
0.001	2.0	100	50
1	2.5	200	100
		400	200
		500	250
		800	500
		1000	750
			1000

$$W_i^N = \pi\left(\frac{1-r_i^2}{N+1}\right), \quad (i = 1, \ldots N). \tag{26c}$$

Note that there is $N + 1$ equation to determine the N unknowns $g(r_i)$ in Eq. (25a). Since the extra equation is used to normalize the interval of integration, it is enough to choose only N of the $N + 1$ possible collocation points [37]. Thus, Eqs. (25a) and (25b) give $N + 1$ equations to determine the $N + 1$ unknowns, which are $g(r_i)$ and a. The system of equations is linear in terms of the $g(r_i)$ but highly nonlinear in variable a. Therefore, an iterative method is used to obtain the unknown.

3 Application of the artificial neural network

Artificial neural networks are computing systems that digitized the human brain. ANNs include methods, tools, and systems that simulate brain activity to solve problems. ANN can make decisions about the relationships between variables and reach a conclusion. ANNs learning process takes place in two ways: supervised and unsupervised. The MLP is the most popular supervised learning approach because of its clear architecture and comparably simple algorithm [38].

The MLP consists of neurons arranged in layers, and each neuron is independent in its own layer but is connected to all neurons in the next layer with weights [39]. The MLP performs with two functions: summation and activation [40]. Inputs are multiplied by the connection weights first summed and then modified by the activation function during training to generate best output [41].

A neural network consists of three layers; input layer, one or more hidden layers, and an output layer. The input layer receives data from the external environment and distributes the inputs to subsequent layers. The hidden layer processes input information and transmits it to output layer.

3.1 Network architecture

In the present study, the input data used for the training of the network were obtained from theoretical solutions. The input layer consists of four different processing elements. These are as follows,

R/h: Rigid punch radius
β: Stiffness parameter for FG layer

$\frac{\mu_0}{P/h}$: Load factor

κ: Material constant

The output layer consists of two different processing elements. These are as follows:

- $\frac{p^{max}(x)}{P/h}$: Maximum contact pressure between the rigid punch and the FG layer
- a/h: Half contact length between rigid circular punch and FG layer

A total of 190 patterns which are different combinations of the values in Table 1 are solved theoretically to create the training set. The input and output values of each pattern were normalized in the [0.1–0.9] range.

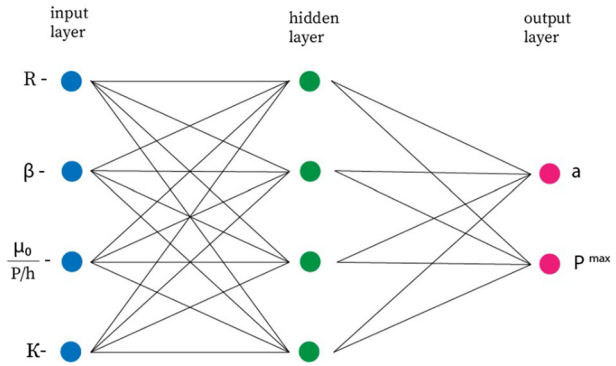

Fig. 2 System architecture

The number of connections has a significant effect on network performance. Excessive number of neurons in the hidden layer can hinder the learning process and over train [41]. The less numbers may cause difficulties in learning process [42]. The number of neurons in the hidden layer can be found through trial-and-error methods [43]. In this study, 1–15 units were used in the hidden layer to find the optimum number of neurons. The weights were initialized into random values between 0.0001 and 0.001. Then, the appropriateness values of the error functions (the sum of squares and entropy) were compared.

In this work, six mathematical functions (Identity, Logistic sigmoid, Hyperbolic tangent, Exponential, SoftMax, and Gaussian) were tested. Figure 2 demonstrates the architecture of the MLP. The network was designed with the Broyden–Fletcher–Goldfarb–Shanno (BFGS) algorithm. Finally, the neural network architecture was developed with the variables selected in the previous step, and 5000 networks were trained and retained. The network model was performed in Statistica software 12 using the neural network module. The program code was rewritten in C++ to calculate the contact area and contact stress.

4 Finite element analysis study

There are limited analysis techniques about FGM contact problems despite their practical importance in engineering applications. Most of the analyses of involving structural elements with FGMs are analytically based on theory of elasticity solution techniques. Finite element analysis, one of the effective numerical solution alternatives, is chosen in line with reliable results for the analysis of such structural problems in the literature. In recent years, various methods have been used to solve difficult and complex engineering problems. Numerical analysis methods are especially preferred. One of the most widely used methods is the finite element method. In finite elements, solutions are made on a large number of divided elements instead of the whole part and the result is reached. There are many computer programs based on the finite element method principle. In this study, the finite element model of the problem was made using ANSYS Mechanical APDL Product Launcher program [44].

Verification of the developed analytical method is provided by utilizing the computational results for contacts and FG layer generated through the general-purpose finite element analysis software ANSYS Mechanical APDL. The finite element model of the problem is defined as the two-dimensional plane-strain contact problem. The geometric model was created with ANSYS standard menu tools. 39,910 quadrilateral 8-node 213,930 PLANE 183 elements, which are preferred in problem solutions such as elasticity and plasticity, were used as element type in the meshing step. The PLANE 183 element has 8 nodes and 2 degrees of freedom and has 8 nodes—4 corner and 4 mid-nodes with 2 translational degrees of freedom in the nodal *x, y* directions. In the meshing process, each line is divided into 0.05-unit intervals. In the process of dividing into finite elements, when the length of the mesh element is decreased, there is an increase in the processing time, and when the interval is increased, the results are distorted.

In this problem, there is contact between the layer and the rigid punch. Contact pairs between the punch-layer are defined. These pairs are divided into contact and target elements. The contact between the layer and the rigid punch is defined by contact element as CONTA169 and target element as TARGE172 elements available in ANSYS Mechanical APDL. As TARGE169, it would be appropriate to choose more rigid, flat-surfaced elements with a larger surface than the contact element. In addition, while choosing the formulation

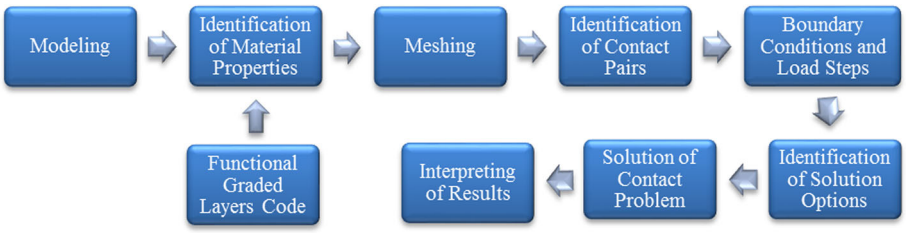

Fig. 3 Summarized steps of the contact analysis

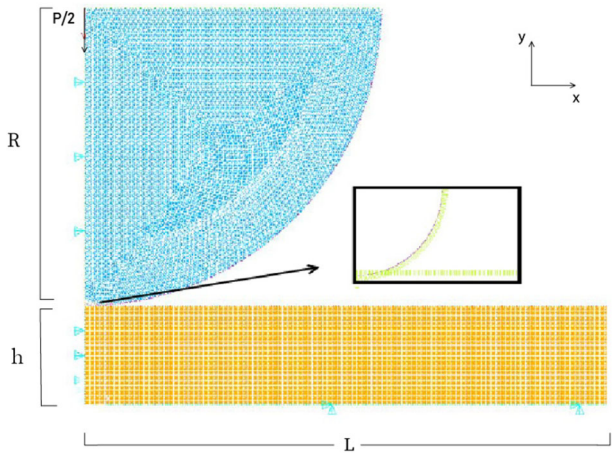

Fig. 4. 2-D model of FG layer contact problem

to be used in the contact area, the mathematical method that will provide the appropriate contact conditions is also decided. In this study, the augmented Lagrangian method, which uses the total potential energy theorem as the contact algorithm, was preferred. A total of 334 lines contact elements exist in the finite element model.

The material properties of the functionally graded layer of the model are taken to be elastic and isotropic. The system is physically symmetrical in terms of geometric, material properties, and loading. Therefore, half of the problem geometry can be modeled because the system is symmetrical.

Finite element solution of FGMs' contact problems is very complex, so some commercial FEA software does not allow material properties to be changed spatially. The available software packages like ANSYS do not automatically provide such capabilities and require the development of user defined subroutines and functions. The procedure is as follows. The geometry is modeled and meshed with appropriate structural elements. Modeling the functionally graded layer using the finite element method is quite complex. Simultaneous thickness changes should be considered in this program. First, function code was developed to define the functionally graded layers by changing the material properties of the layers along the layer and added to the program's log files with the extension of "log." With respect to the change in the properties of the FGM material in accordance with the layer thickness, the function for material properties is used to define the material. Then, contact is defined, and the structural model is solved to obtain the contact response. The summarized methodology flowchart to solve contact problems involving inhomogeneous materials (FGMs) by FEM is represented schematically in Fig. 3.

In the analyses, as geometric properties length of the layer in x direction is taken as $L = 10\ m$, thickness of the lower layer in y direction is taken as $h = 1\ m$. Besides, other parameters (R, P, κ, β) vary according to the desired solution. The Young's modulus of the element used in layer is calculated according to the grade function $\mu(y) = \mu_0.e^{(\beta y)}$. ANSYS does not include any specified module to incorporate functional grading of material properties. For this reason, as an original contribution to study, a function code was developed to define the functionally graded layers by changing the material properties of the layers along the y axis and added to the log files of the program. The contact problem meshed model in ANSYS software is shown in Fig. 4. The deformed shape that occurred after analysis of these models is shown in Fig. 5.

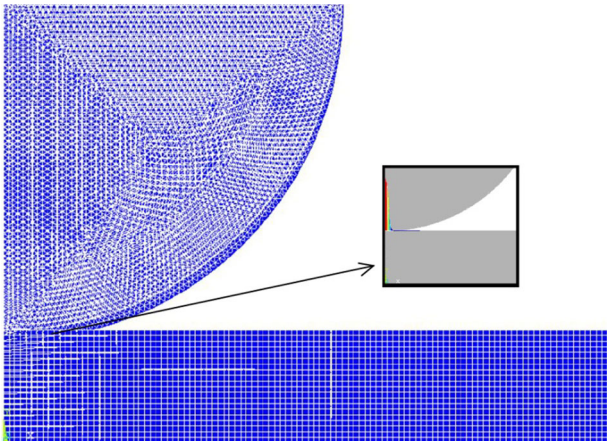

Fig. 5 Deformed shape of model in ANSYS

5 Numerical results

In this chapter of the study, the contact lengths and contact stresses between the FG layer and rigid punch are calculated for different material, loading, and geometric values. Results are shown in graphics and tables. The conclusions and recommendations drawn from this study are given as follows.

In this study, the potential of MLP to predict contact pressures and contact areas was evaluated. The results showed that MLP-based networks can accurately predict contact pressures and contact areas. This analysis provides quick and simple predictions. The networks, with the error term "sos" produced superior results. The hidden layer configurations ranged between 14 and 15 units. Tanh in the hidden layer and Exponential in the output layer were determined as the activation functions that produced the most successful results. Table 2 demonstrates the characteristics of the best neural networks for recognizing output elements.

This section presents the numerical results for contact area and contact stress distribution of the FG layer due to frictionless contact of a rigid cylindrical punch. The values μ_0 and h should be considered to be fixed, and they are related to more than one dimensionless quantities.

Therefore, the effects of the non-homogeneity parameter, load factor, the radius of rigid punch, and material constant on the contact pressures and the contact lengths are examined in Figs. 6, 7, 8, 9, 10 and Tables 3, 4, 5. In the solutions, $\beta = -1$, $\beta = 0.001$, $\beta = 1$ values are used for the non-homogeneity parameter. The various dimensionless quantities mentioned in the tables and graphics are given below:

$\frac{p^{max}(x)}{(P/h)}$: Maximum contact stress between the rigid punch and the FG layer
a/h: Half contact area between rigid circular punch and FG layer
R/h: Ratio of rigid punch radius to FG layer height
β: Non-homogeneity parameter for FG layer
$\frac{\mu_0}{(P/h)}$: Load factor
κ: Material constant

The relative error is determined as follows:

$$e_{\text{MLP/FEM}} = \left| \frac{E_{\text{analytical}} - E_{\text{numerical}}}{E_{\text{analytical}}} \right| * 100 \tag{27}$$

where $E_{\text{analytical}}$ and $E_{\text{numerical}}$ are the analytical, MLP and FEM, solutions of the *a/h* and $p^{\max}(x)/(P/h)$ [45].

The maximum relative errors of the contact areas (*a/h*) are calculated as $e_{\text{MLP}} = 3.72\%$ and $e_{\text{FEM}} = 4.51\%$. The average relative errors of the (*a/h*) are calculated as $e_{\text{MLP}} = 0.62\%$ and $e_{\text{FEM}} = 1.26\%$ (Fig. 6).

Tables 3, 4, 5 show the variation of the contact area with non-homogeneity parameter β. $\beta h > 0$ indicates that the rigidity of the top surface is higher than bottom surface of the layer. On the contrary when $\beta h < 0$, rigidity is the opposite of the first case. When is β is higher, the contact area a/h decreases. Tables 3, 4, 5 also show variation contact area depending on load factor $\mu_0/(P/h)$, radius of rigid punch R/h, and material constant κ. Since increasing load factor $\mu_0/(P/h)$ corresponds to decreasing of applied concentrated load P, contact area (a/h) decreases (Table 3). Contact area (a/h) increases with increasing of radius of rigid punch

Table 2 The characteristics of artificial networks that recognize output elements

Network	MLP	Error in learning (%)	Error in testing (%)	Error in validation (%)	Learning algorithm	Error function	Activation function in hidden layer	Activation function in output layer
N1	4–14–1	3.43	0	0	BFGS298	SOS	Tanh	Exponential
N2	4–15–1	0	0	0	BFGS405	SOS	Tanh	Exponential

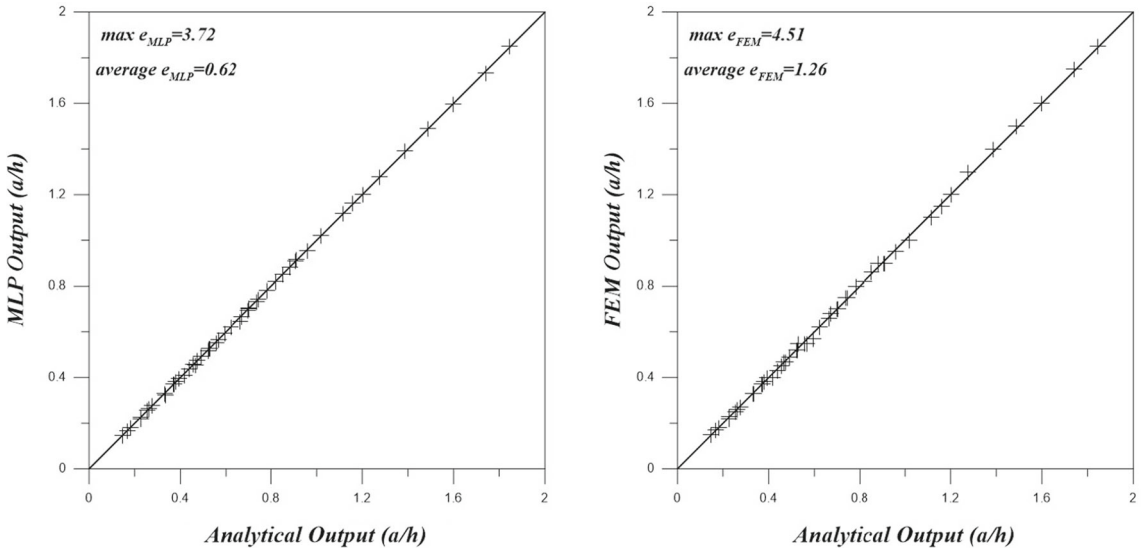

Fig. 6 Comparison of contact areas obtained from MLP and FEM with analytical results

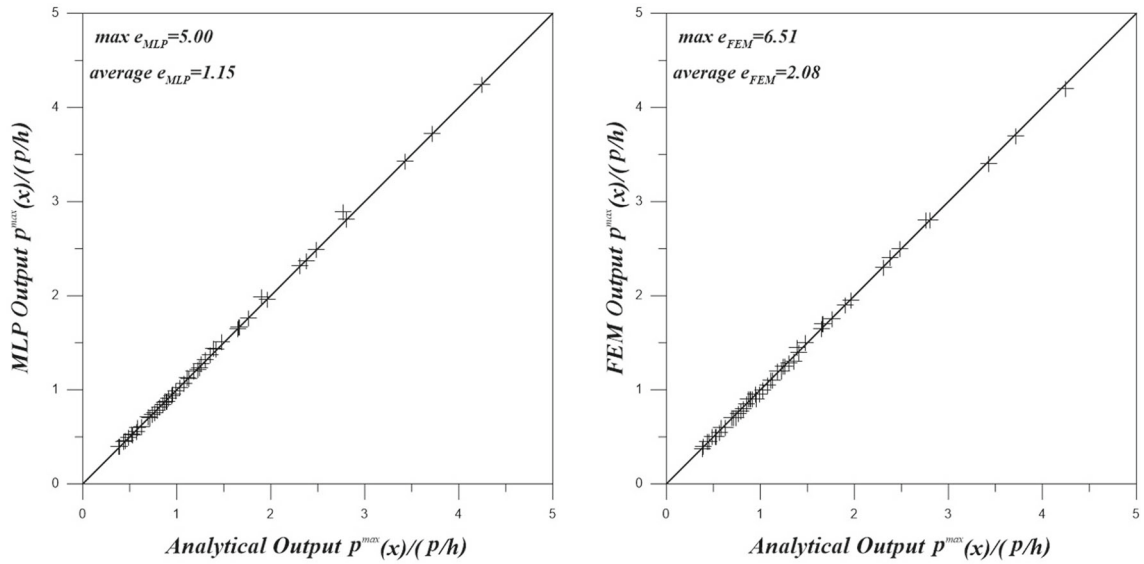

Fig. 7 Comparison of contact stresses obtained from MLP and FEM with analytical results

R/h (Table 4). In Table 5, the contact area (a/h) is analyzed depending on the various value quantities of the materials constant κ. In Table 5, it is seen that contact width (a/h) increases with increasing material constant κ. Increasing of κ corresponds to decreasing of Poisson ratio ν.

The maximum relative errors of maximum contact stress $p^{\max}(x)/(P/h)$ are calculated as $e_{\text{MLP}} = 5.00\%$ and $e_{\text{FEM}} = 6.51\%$. The average relative errors of the $p^{\max}(x)/(P/h)$ are calculated as $e_{\text{MLP}} = 1.15\%$ and $e_{\text{FEM}} = 2.08\%$ (Fig. 7).

Figures 8, 9, 10 illustrate the effect of the relative in non-homogeneity parameter on the contact stress on the top of the FG layer. Figure 8 shows the effect of some values of load factor (75, 150, 300, 600, 700 and 900) on $p^{\max}(x)/(P/h)$ dimensionless maximum contact. As load factor increases $\mu_0/(P/h)$, dimensionless maximum contact stress increases. Also contact stresses increases when non-homogeneity parameter β increases.

Figure 9 shows $p^{\max}(x)/(P/h)$ maximum contact stress depending on the radius of rigid punch *R/h* and non-homogeneity parameter β. In Fig. 9, $\mu_0/(P/h) = 100$ and $\kappa = 2$ are fixed and maximum contact stress for $R/h = 25$, $R/h = 150$, $R/h = 250$ $R/h = 600$, $R/h = 750$ and $R/h = 900$ is given. As R/h increases,

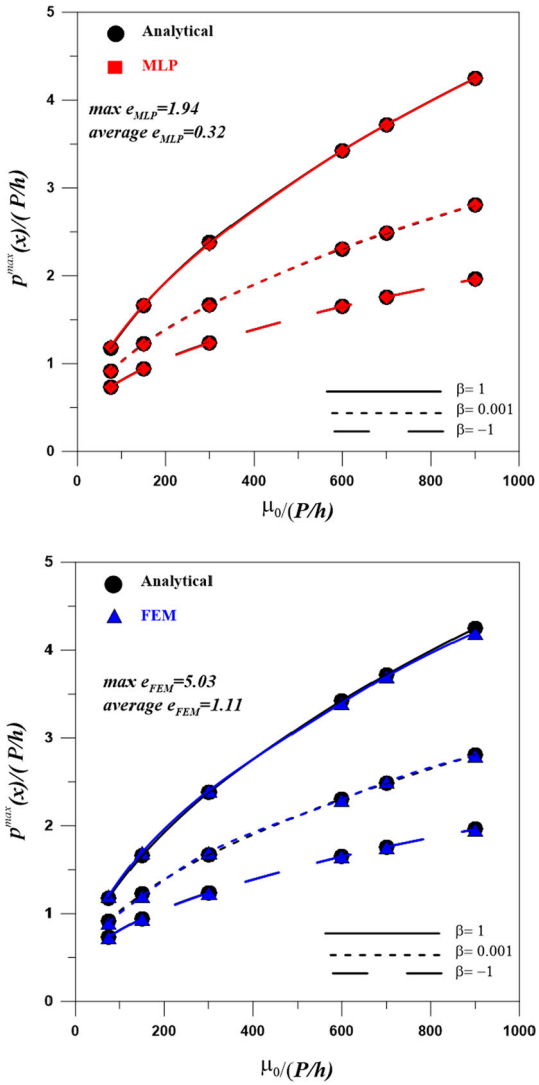

Fig. 8 Variations of the $p^{\max}(x)/(P/h)$ with $\mu_0/(P/h)$, $(R/h = 100, \kappa = 2)$

size of the contact area increases, so the applied load distributes a much larger area. Therefore, maximum contact stress decreases. With increasing non-homogeneity parameter β, contact stresses increase.

Figure 10 shows $p^{\max}(x)/(P/h)$ maximum contact stress depending on material constant κ and non-homogeneity parameter β. In Fig. 10, $\mu_0/(P/h) = 100$ and $R/h = 100$ are fixed and maximum contact stress for κ=1.5, κ=1.75, κ=2, κ=2.25 and κ=2.5 is given. As material constant increases, maximum contact stress decreases. With increasing non-homogeneity parameter β, contact stresses increasing.

6 Conclusions

Contact area and contact stress are important parameters in the solution of FGM contact problems in the engineering field. Several methods and analysis can be carried out to find these values. It is important for researchers to find the most practical and reliable method.

The analytical solution based on the theory of elasticity in FGM contact problems gives exact results. The contact area and contact stress results obtained by MLP and FEM methods were compared with analytical results and their power and viability were examined.

In this study, a frictionless contact problem between a rigid punch and functionally graded (FG) layer, which is bonded to a rigid foundation on its bottom surface was analytically analyzed with the theory of elasticity

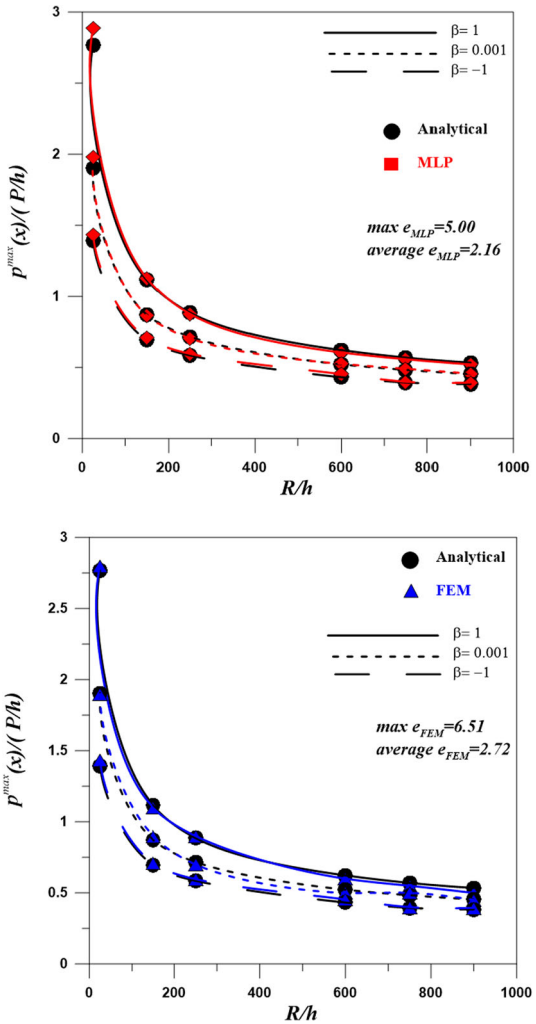

Fig. 9 Variations of the $p^{\max}(x)/(P/h)$ with *R/h*, $(\mu_0/(P/h) = 100, \kappa = 2)$

and numerically analyzed with MLP and FEM. In the examination of the problem, unknown contact area and maximum contact stress were calculated using three different methods. The ability of the MLP and FEM to determine the contact area and maximum contact stress is evaluated by emphasizing the approximation to the numerical results obtained. The numerical values for the Contact areas and maximum contact stresses between the FG layer and rigid stamp are calculated for different material, loading, and geometric properties. It was observed that the software and MLP technique are general-purposes and can be used in all contact geometry, material properties, and mesh types with minor changes. It is also possible to say that by using the developed FEM and MLP model, acceptable results can be obtained in a relatively short period of time, without the need for long and complex mathematical expressions of theoretical solutions. Besides, the results obtained at the end of the study are summarized below,

- When the value of non-homogeneity parameter (β) is increased, the maximum contact stresses increase, and the contact areas decrease. If the value (β) increases in the positive direction, the flexural stiffness of the FG layer and contact areas increase. On the other hand, negative (β) values lead to reduced flexural stiffness of the FG layer and to forming smaller contact areas.
- When the results of contact areas and maximum contact stresses obtained by using numerical solution methods (FEM and MLP) are compared with analytical results, the error rates were found to be very low.
- This work shows that the MLP and FEM were able to obtain the contact areas and contact stress for the functionally graded material contact problem, saving significant time.

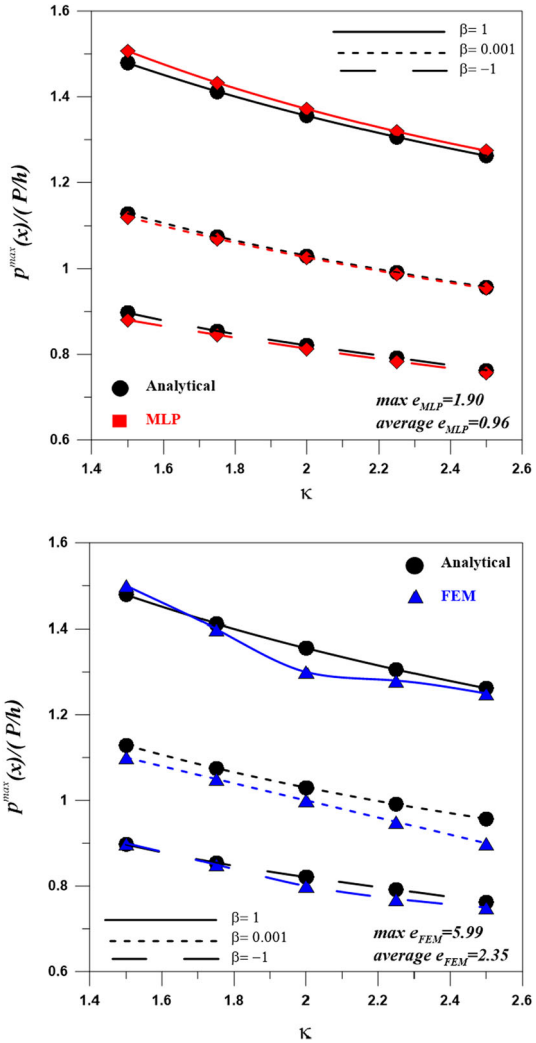

Fig. 10 Variations of the $p^{\max}(x)/(P/h)$ with κ, $(\mu_0/(P/h)100,\ R/h = 100)$

Table 3 Change of contact areas (a/h) with $\mu_0/(P/h)$ value $(R/h = 100, \kappa = 2)$

$\frac{\mu_0}{P/h}$	a/h					
	β	Analytical	MLP	FEM	e_{MLP}	e_{FEM}
75	1	0.5253	0.5286	0.5200	0.62	1.01
	0.001	0.7025	0.7051	0.7000	0.38	0.36
	−1	0.9125	0.918	0.9000	0.60	1.37
150	1	0.3742	0.3714	0.3700	0.74	1.12
	0.001	0.5215	0.5163	0.5200	0.99	0.29
	−1	0.6997	0.694	0.7000	0.87	0.04
300	1	0.2626	0.2632	0.2600	0.21	0.99
	0.001	0.3813	0.3814	0.3800	0.04	0.34
	−1	0.5279	0.529	0.5500	0.16	4.19
600	1	0.1830	0.1819	0.1800	0.60	1.64
	0.01	0.2752	0.2763	0.2700	0.41	1.89
	−1	0.3936	0.396	0.4000	0.57	1.63
700	1	0.1689	0.1671	0.1700	1.09	0.65
	0.01	0.2556	0.2564	0.2500	0.31	2.19
	−1	0.3682	0.370	0.3700	0.43	0.49
900	1	0.1481	0.1459	0.1500	1.46	1.28
	0.01	0.2264	0.2269	0.2200	0.23	2.83
	−1	0.3298	0.330	0.3300	0.15	0.06

Table 4 Change of contact areas (*a/h*) with (*R/h*) value ($\mu_0/(P/h) = 100, \kappa = 2$)

R/h	*a/h*					
	β	Analytical	MLP	FEM	e_{MLP}	e_{FEM}
25	1	0.2262	0.2192	0.2300	3.09	1.68
	0.001	0.3335	0.3211	0.3300	3.72	1.05
	−1	0.4680	0.4550	0.4700	2.84	0.43
150	1	0.5553	0.5513	0.5500	0.72	0.95
	0.001	0.7378	0.7341	0.7500	0.50	1.65
	−1	0.9581	0.9550	0.9500	0.28	0.85
250	1	0.7015	0.7018	0.7000	0.04	0.21
	0.001	0.9081	0.9099	0.9000	0.20	0.89
	−1	1.1594	1.1640	1.1500	0.39	0.81
600	1	1.0196	1.0202	1.0000	0.06	1.92
	0.01	1.2760	1.2780	1.3000	0.16	1.88
	−1	1.5986	1.5970	1.6000	0.13	0.09
750	1	1.1172	1.1177	1.1000	0.05	1.54
	0.01	1.3880	1.3916	1.4000	0.26	0.86
	−1	1.7419	1.7320	1.7500	0.58	0.47
900	1	1.2020	1.2025	1.2000	0.04	0.17
	0.01	1.4858	1.4897	1.5000	0.26	0.96
	−1	1.8442	1.8500	1.8500	0.29	0.31

Table 5 Change of contact areas (*a/h*) with (κ) value ($\mu_0/(P/h)100$, *R/h = 100*)

κ	*a/h*					
	β	Analytical	MLP	FEM	e_{MLP}	e_{FEM}
1.5	1	0.4189	0.4112	0.4000	1.85	4.51
	0.001	0.5676	0.5655	0.5500	0.37	3.10
	−1	0.7438	0.7420	0.7500	0.20	0.83
1.75	1	0.4387	0.4363	0.4300	0.55	1.98
	0.001	0.5956	0.5943	0.5700	0.22	4.30
	−1	0.7830	0.7810	0.8000	0.20	2.17
2.00	1	0.4574	0.4571	0.4500	0.06	1.62
	0.001	0.6222	0.6202	0.6200	0.33	0.35
	−1	0.8203	0.8180	0.8200	0.31	0.04
2.25	1	0.4750	0.4755	0.4700	0.11	1.05
	0.01	0.6647	0.6443	0.6600	3.07	0.71
	−1	0.8529	0.8510	0.8600	0.17	0.83
2.50	1	0.4917	0.4927	0.4900	0.20	0.35
	0.01	0.6702	0.6672	0.6800	0.45	1.46
	−1	0.8823	0.8830	0.9000	0.05	2.01

Declarations

Conflict of interest The authors declare no conflicts of interest.

Consent to participate No external participants have contributed to the work discussed in this manuscript.

Consent for publication The authors give their full consent to the editor to publish this article if accepted.

Ethical approval The authors declare that the research was conducted according to the ethical standards.

Human and animal study This article does not contain any studies with human or animal subjects.

Appendix 1

$$
\begin{aligned}
A_1 =& -(P(D_2m_3e^{hn_2} - D_2m_4e^{hn_2} - D_3m_2e^{hn3} + D_3m_4e^{hn_3} + D_4m_2e^{hn_4} - D_4m_3e^{hn_4}))/\Delta\\
A_2 =& (P(D_1m_3e^{hn_1} - D_1m_4e^{hn_1} - D_3m_1e^{hn3} + D_4m_1e^{hn_4} + D_3m_4e^{hn_3} - D_4m_3e^{hn_4}))/\Delta\\
A_3 =& -(P(D_1m_2e^{hn_1} - D_2m_1e^{hn_2} - D_1m_4e^{hn_1} + D_2m_4e^{hn_2} + D_4m_1e^{hn_4} - D_4m_2e^{hn_4}))/\Delta\\
A_4 =& (P(D_1m_2e^{hn_1} - D_1m_3e^{hn_1} - D_2m_1e^{hn_2} + D_2m_3e^{hn_2} + D_3m_1e^{hn_3} - D_3m_2e^{hn_3}))/\Delta\\
\Delta A =& (e^{hn_1}e^{hn_2}(C_1D_2m_3 - C_2D_1m_3 - C_1D_2m_4 + C_2D_1m_4)\\
&+ e^{hn_1}e^{hn_3}(-C_1D_3m_2 + C_3D_1m_2 + C_1D_3m_4 - C_3D_1m_4)\\
&+ e^{hn_1}e^{hn_4}(C_1D_4m_2 - C_4D_1m_2 - C_1D_4m_3 + C_4D_1m_3)\\
&+ e^{hn_2}e^{hn_3}(C_2D_3m_1 - C_3D_2m_1 - C_2D_3m_4 + C_3D_2m_4)\\
&+ e^{hn_2}e^{hn_4}(-C_2D_4m_1 + C_4D_2m_1 + C_2D_4m_3 - C_4D_2m_3)\\
&+ e^{hn_3}e^{hn_4}(C_3D_4m_1 - C_4D_3m_1 - C_3D_4m_2 + C_4D_3m_2))
\end{aligned}
$$

Appendix 2

$$
\begin{aligned}
N(x,t) =& \int_0^\infty \frac{\xi(\kappa-1)}{2\Delta A}\{[e^{(n_1+n_2)h}(m_1m_4D_2 - m_1m_3D_2 + m_2m_3D_1 - m_2m_4D_1)\\
&+ e^{(n_1+n_3)h}(m_1m_2D_3 - m_1m_4D_3 - m_2m_3D_1 + m_3m_4D_1)\\
&+ e^{(n_1+n_4)h}(-m_1m_2D_4 + m_1m_3D_4 + m_2m_4D_1 - m_3m_4D_1)\\
&+ e^{(n_2+n_3)h}(-m_1m_2D_3 + m_2m_4D_3 + m_1m_3D_2 - m_3m_4D_2)\\
&+ e^{(n_2+n_4)h}(m_1m_2D_4 - m_2m_3D_4 - m_1m_4D_2 + m_3m_4D_2)\\
&+ e^{(n_3+n_4)h}(-m_1m_3D_4 + m_2m_3D_4 + m_1m_4D_3 - m_2m_4D_3) + \frac{\kappa+1}{8}]\}\sin\xi(t-x)\mathrm{d}\xi
\end{aligned}
$$

Appendix 3

$$
\begin{aligned}
k(s,r) =& \int_0^\infty \frac{\frac{z}{h}(\kappa-1)}{2\Delta A}\{[e^{(n_1+n_2)h}(m_1m_4D_2 - m_1m_3D_2 + m_2m_3D_1 - m_2m_4D_1)\\
&+ e^{(n_1+n_3)h}(m_1m_2D_3 - m_1m_4D_3 - m_2m_3D_1 + m_3m_4D_1)\\
&+ e^{(n_1+n_4)h}(-m_1m_2D_4 + m_1m_3D_4 + m_2m_4D_1 - m_3m_4D_1)\\
&+ e^{(n_2+n_3)h}(-m_1m_2D_3 + m_2m_4D_3 + m_1m_3D_2 - m_3m_4D_2)\\
&+ e^{(n_2+n_4)h}(m_1m_2D_4 - m_2m_3D_4 - m_1m_4D_2 + m_3m_4D_2)\\
&+ e^{(n_3+n_4)h}(-m_1m_3D_4 + m_2m_3D_4 + m_1m_4D_3 - m_2m_4D_3) + \frac{\kappa+1}{8}]\}\sin z\left(\frac{ar}{h} - \frac{as}{h}\right)\mathrm{d}z
\end{aligned}
$$

References

1. Öner, E., Birinci, A.: Investigation of the solution for discontinuous contact problem between a functionally graded (FG) layer and homogeneous half-space. Arch. Appl. Mech. **90**, 2821–2823 (2020). https://doi.org/10.1007/s00419-020-01777-1
2. Matysiak, S.J., Pauk, V.J.: Plane contact problem for periodic laminated composite involving frictional heating. Arch. Appl. Mech. **66**, 82–89 (1995). https://doi.org/10.1007/BF00786691
3. Naebe, M., Shirvanimoghaddam, K.: Functionally graded materials: a review of fabrication and properties. Appl. Mater. Today **5**, 223–245 (2016). https://doi.org/10.1016/j.apmt.2016.10.001
4. Yarimpabuc, D., Eker, M., Celebi, K.: Mechanical behavior of functionally graded pressure vessels under the effect of Poisson's ratio. Euro. Mech. Sci. **2**(2), 52–59 (2018). https://doi.org/10.26701/ems.360134

5. Cannillo, V.L., Lusvarghi, C., Siligardi, S.A.: Prediction of the elastic properties profile in glass-alumina functionally graded materials. J. Eur. Ceram. Soc. **27**(6), 2393–2400 (2007). https://doi.org/10.1016/j.jeurceramsoc.2006.09.009
6. Jha, D.K., Kant, T., Singh, R.K.: Critical review of recent research on functionally graded plates. Compos. Struct. **96**, 833–849 (2013). https://doi.org/10.1016/j.compstruct.2012.09.001
7. Cheraghi, N., Lezgy-Nazargah, M., Etemadi, E.: Free vibration analysis of functionally graded magneto-electro-elastic plates resting on elastic foundations with considering interfacial imperfections. Modares Mech. Eng. **19**(3), 655–663 (2019)
8. Bayat, Y., Ghannad, M., Torabi, H.: Analytical and numerical analysis for the FGM thick sphere under combined pressure and temperature loading. Arch. Appl. Mech. **82**, 229–242 (2012). https://doi.org/10.1007/s00419-011-0552-x
9. Van Do, V.N., Chang, K.H., Lee, C.H.: Post-buckling analysis of FGM plates under in-plane mechanical compressive loading by using a mesh-free approximation. Arch. Appl. Mech. **89**, 1421–1446 (2019). https://doi.org/10.1007/s00419-019-01512-5
10. Adiyaman, G., Birinci, A., Öner, E., Yaylacı, M.: Receding contact problem between a functionally graded layer and two homogeneous quarter planes. Acta Mech. **227**, 1753–1766 (2016). https://doi.org/10.1007/s00707-016-1580-y
11. Yan, J., Mi, C.: On the receding contact between a homogeneous elastic layer and a half-plane substrate coated with FGMs. Int. J. Comput. Methods **15**(1), 1–21 (2018). https://doi.org/10.1142/S0219876218440085
12. Comez, I.: Continuous and discontinuous contact problem of a functionally graded layer pressed by a rigid cylindrical punch. Eur. J. Mech. A Solids **73**, 437–448 (2019). https://doi.org/10.1016/j.euromechsol.2018.10.009
13. Yaylacı, M., Terzi, C., Avcar, M.: Numerical analysis of the receding contact problem of two bonded layers resting on an elastic half plane. Struct. Eng. Mech. (2019). https://doi.org/10.12989/sem.2019.72.6.000
14. Yaylacı, M., Avcar, M.: Finite element modeling of contact between an elastic layer and two elastic quarter planes. Comput. Conc. **26**(2), 107–114 (2020). https://doi.org/10.12989/cac.2020.26.2.000
15. Beheshti-Aval, S.B., Lezgy-Nazargah, M.: A coupled refined high-order global-local theory and finite element model for static electromechanical response of smart multilayered/sandwich beams. Arch. Appl. Mech. **82**, 1709–1752 (2012). https://doi.org/10.1007/s00419-012-0621-9
16. Izadi, M.H., Hosseini-Hashemi, S., Korayem, M.H.: Analytical and FEM solutions for free vibration of joined cross-ply laminated thick conical shells using shear deformation theory. Arch. Appl. Mech. **88**, 2231–2246 (2018). https://doi.org/10.1007/s00419-018-1446-y
17. Lezgy-Nazargah, M., Vidal, P., Polit, O.: A quasi-3D finite element model for the analysis of thin-walled beams under axial–flexural–torsional loads. Thin Walled Struct. **164**, 107811 (2021). https://doi.org/10.1016/j.tws.2021.107811
18. Haeri, H., Sarfarazi, V., Ebneabbasi, P., Maram, A.N., Shahbazian, A., Marji, M.F., Mohamadi, A.R.: XFEM and experimental simulation of failure mechanism of non-persistent joints in mortar under compression. Constr. Build. Mater. (2020). https://doi.org/10.1016/j.conbuildmat.2019.117500
19. Haeri, H., Maleki, M., Shahvali, H., Sarfarazi, V., Marji, M.F.: Evaluating the fragility curve in steel–concrete structure undergoing seismic progressive collapse by Finite Element Method. Iran J. Sci. Technol. Trans. Civ. Eng. (2021). https://doi.org/10.1007/s40996-021-00764-y
20. Fu, J., Haeri, H., Sarfarazi, V., Asgari, K., Ebneabbasi, P., Marji, M.F., Guo, M.: Extended finite element method simulation and experimental test on failure behavior of defects under uniaxial compression. Mech. Adv. Mater. Struct. (2021). https://doi.org/10.1080/15376494.2021.1989730
21. Sarfarazi, V., Abad, M.B., S.: Failure pattern of perpendicular non-persistent joints beneath the point load of bm's cutter using experimental test and Finite Element Method. Miner. Resour. Eng. **5**(4), 73–94 (2020). https://doi.org/10.30479/jmre.2020.11307.1299
22. Oner, E., Yaylacı, M., Birinci, A.: Analytical solution of a contact problem and comparison with the results from FEM. Struct. Eng. Mech. **54**(4), 607–622 (2015). https://doi.org/10.12989/sem.2015.54.4.607
23. Lezgy-Nazargah, M., Meshkani, Z.: An efficient partial mixed finite element model for static and free vibration analyses of FGM plates rested on two-parameter elastic foundations. Struct. Eng. Mech. **66**(5), 665–676 (2018). https://doi.org/10.12989/SEM.2018.66.5.665
24. Yaylacı, M., Öner, E., Birinci, A.: Comparison between analytical and ANSYS calculations for a receding contact problem. J. Eng. Mech. **140**(9), 4014070 (2014). https://doi.org/10.1061/(ASCE)EM.1943-7889.0000781
25. Yaylacı, M., Adıyaman, E., Öner, E., Birinci, A.: Examination of analytical and finite element solutions regarding contact of a functionally graded layer. Struct. Eng. Mech. **76**(3), 325–336 (2020). https://doi.org/10.12989/sem.2020.76.3.325
26. Yaylacı, M., Adıyaman, E., Öner, E., Birinci, A.: Investigation of continuous and discontinuous contact cases in the contact mechanics of graded materials using analytical method and FEM. Comput. Conc. **27**, 199–210 (2021). https://doi.org/10.12989/CAC.2021.27.3.199
27. Katsikadelis, J., Tsiatas, G.: Buckling load optimization of beams. Arch. Appl. Mech. **74**, 790–799 (2005). https://doi.org/10.1007/s00419-005-0402-9
28. Sarmadi, H., Entezami, A.: Application of supervised learning to validation of damage detection. Arch. Appl. Mech. **91**, 393–410 (2021). https://doi.org/10.1007/s00419-020-01779-z
29. Hattori, G., Serpa, A.L.: Contact stiffness estimation in ANSYS using simplified models and artificial neural networks. Finite Elem. Anal. Des. **97**, 43–53 (2015). https://doi.org/10.1016/j.finel.2015.01.003
30. Serafińska, A., Graf, W., Kaliske, M.: Artificial neural networks-based friction law for elastomeric materials applied in finite element sliding contact simulations. Compl. Compl. Algorith. Data Driv. Model Learn. Sci. Eng. (2018). https://doi.org/10.1155/2018/4396758
31. Górski, J., Klepka, A., Dziedziech, K., Mrówka, J., Radecki, R., Dworakowski, Z.: Identification of the stick and slip motion between contact surfaces using artificial neural networks. Nonlinear Dyn. **100**, 225–242 (2020). https://doi.org/10.1007/s11071-020-05515-8
32. Uzun Yaylacı, E., Yaylacı, M., Ölmez, H., Birinci, A.: Artificial neural network calculations for a receding contact problem. Comput. Conc. **25**, 6 (2020). https://doi.org/10.12989/cac.2020.25.6.000

33. Yaylacı, M., Eyüboğlu, A., Adıyaman, G., Uzun Yaylacı, E., Öner, E., Birinci, A.: Assessment of different solution methods for receding contact problems in functionally graded layered mediums. Mech. Mater. (2021). https://doi.org/10.1016/j.me)chmat.2020.103730
34. Yaylacı, M., Yaylı, M., Uzun Yaylacı, E., Ölmez, H., Birinci, A.: Analyzing the contact problem of a functionally graded layer resting on an elastic half plane with theory of elasticity, finite element method and multilayer perceptron. Struct. Eng. Mech. **78**, 585–597 (2021). https://doi.org/10.12989/sem.2021.78.5.585
35. Öner, E., Şengül Şabano, B., Uzun Yaylacı, E., Adıyaman, G., Yaylacı, M., Birinci, A.: On the plane receding contact between two functionally graded layers using computational, finite element and artificial neural network methods. ZAMM (2022). https://doi.org/10.1002/zamm.202100287
36. Erdogan, F.: Mixed boundary value problems in mechanics. In: Nemat-Nasser, S. (ed.) Mechanics Today 4. Pergamon Press, New York (1978)
37. Krenk, S.: On quadrature formulas for singular integral equations of the first and the second kind. Q. Appl. Math. **33**, 225–232 (1975)
38. Yan, H., Jiang, Y., Zheng, J., Peng, C., Li, Q.: A multilayer perceptron based medical decision support system for heart disease diagnosis. Exp. Syst. Appl. **30**(2), 272–281 (2006). https://doi.org/10.1016/j.eswa.2005.07.022
39. Cakiroglu, E., Comez, I., Erdol, R.: Application of artificial neural networks to a double receding contact problem with a rigid stamp. Struct. Eng. Mech. **21**(2), 205–220 (2005). https://doi.org/10.12989/sem.2005.21.2.205
40. Heidari, A.A., Faris, H., Aljarah, I., Mirjalili, S.: An efficient hybrid multilayer perceptron neural network with grasshopper optimization. Soft Comput. **23**(17), 7941–7958 (2019). https://doi.org/10.1007/s00500-018-3424-2
41. Agatonovic-Kustrin, S., Beresford, R.: Basic concepts of artificial neural network (ANN) modeling and its application in pharmaceutical research. J. Pharm. Biomed. Anal. **22**(5), 717–727 (2000). https://doi.org/10.1016/S0731-7085(99)00272-1
42. Buntoung, S., Pariyothon, J., Detkhon, P.: Estimation of atmospheric precipitable water in Thailand using an artificial neural network. NUJST. **29**(2), 11–20 (2020)
43. Subasi, A., Ercelebi, E.: Classification of EEG signals using neural network and logistic regression. Comput. Methods Program. Biomed. **78**(2), 87–99 (2005). https://doi.org/10.1016/j.cmpb.2004.10.009
44. ANSYS Mechanical APDL: ANSYS Contact Technology Guide. Ansys Inc, Canonsburg, Pennsylvania, U.S.A (2013)
45. He, K., Chang, J., Sun, P.D., B, Yin Z, Li D,: Iterative algorithm for the conformal mapping function from the exterior of a roadway to the interior of a unit circle. Arch. Appl. Mech. (2022). https://doi.org/10.1007/s00419-021-02087-w